Ilian A. Radichev,[1,2] Lilia V. Maneva-Radicheva,[1,2] Christina Amatya,[1,2] Camille Parker,[1,2] Jacob Ellefson,[1,2] Clive Wasserfall,[3] Mark Atkinson,[3] Paul Burn,[1,2] and Alexei Y. Savinov[1,2]

Nardilysin-Dependent Proteolysis of Cell-Associated VTCN1 (B7-H4) Marks Type 1 Diabetes Development

Diabetes 2014;63:3470–3482 | DOI: 10.2337/db14-0213

T-cell responses directed against insulin-secreting pancreatic β-cells are the key events highlighting type 1 diabetes (T1D). Therefore, a defective control of T-cell activation is thought to underlie T1D development. Recent studies implicated a B7-like negative costimulatory protein, V-set domain-containing T-cell activation inhibitor-1 (VTCN1), as a molecule capable of inhibiting T-cell activation and, potentially, an important constituent in experimental models of T1D. Here, we unravel a general deficiency within the VTCN1 pathway that is shared between diabetes-prone mice and a subset of T1D patients. Gradual loss of membrane-tethered VTCN1 from antigen-presenting cells combined with an increased release of soluble VTCN1 (sVTCN1) occurs in parallel to natural T1D development, potentiating hyperproliferation of diabetogenic T cells. Mechanistically, we demonstrate that the loss of membrane-tethered VTCN1 is linked to proteolytic cleavage mediated by the metalloproteinase nardilysin. The cleaved sVTCN1 fragment was detected at high levels in the peripheral blood of 53% T1D patients compared with only 9% of the healthy subjects. Elevated blood sVTCN1 levels appeared early in the disease progression and correlated with the aggressive pace of disease, highlighting the potential use of sVTCN1 as a new T1D biomarker, and identifying nardilysin as a potential therapeutic target.

Type 1 diabetes (T1D) is a complex autoimmune disease. Despite extensive research, a detailed understanding of the mechanisms driving diabetogenic autoimmunity is lacking, and a need for reliable biomarkers of this disorder remains pressing. The continuous destruction of insulin-producing β-cells within the pancreatic islets, a hallmark of T1D, is mediated by autoreactive islet–specific T lymphocytes (1,2). In healthy individuals, a small subset of autoreactive T cells escapes thymic negative selection circulating in the periphery in an unprimed naive state (3,4). Failure to silence self-reactive T cells would, therefore, create an autoimmune condition. Accordingly, the activation of islet-specific T cells is the key feature of T1D-associated autoimmunity (5).

T-cell activation entails the integration of two independent signals delivered by antigen-presenting cells (APCs), as follows: antigen-specific and costimulatory. Different costimulatory ligands expressed on APCs bind to T cells, providing for activation or anergy, depending on the nature of the costimulatory signal (6). The "classical" B7-1 and B7-2 costimulatory molecules transduce an activation signal. Lately, several B7-homologous negative costimulatory ligands have been discovered and characterized (7–9).

V-set domain-containing T-cell activation inhibitor-1 (VTCN1), also known as B7-H4, B7S1, and B7x, is a negative costimulatory molecule (8,10) that binds to an unidentified receptor on T cells, delivering downstream signaling through extracellular signal–regulated kinase, Jun NH_2-terminal kinase, and Akt (11). VTCN1 suppresses T-cell responses to antigenic stimulation, decreasing cytokine production and reducing the proliferation of

[1]Sanford Project/Children's Health Research Center at Sanford Research, Sioux Falls, SD
[2]Department of Pediatrics, University of South Dakota School of Medicine, Sioux Falls, SD
[3]Department of Pathology, College of Medicine, University of Florida, Gainesville, FL
Corresponding author: Alexei Y. Savinov, alexei.savinov@sanfordhealth.org.

Received 6 February 2014 and accepted 15 May 2014.
This article contains Supplementary Data online at http://diabetes.diabetesjournals.org/lookup/suppl/doi:10.2337/db14-0213/-/DC1.

both $CD4^+$ and $CD8^+$ T cells (8,10,12). Accumulating evidence indicates that VTCN1-mediated negative costimulation provides a crucial balance between abnormal T-cell activation and anergy. Accordingly, experimental interference with VTCN1 signaling exacerbates multiple autoimmune conditions, as was reported for rheumatoid arthritis (RA) (13) and multiple sclerosis models (10,14).

The persistence of autoreactive T-cell responses during T1D implies that impaired VTCN1 coinhibition may contribute to diabetogenic autoimmunity. Accordingly, matrix surface–bound VTCN1-Ig fusion protein suppressed the proliferation of islet-specific T1D patient-derived T-cell clones, while VTCN1-Ig transfection protected human islets from these clones (15). Furthermore, the treatment of diabetes-susceptible NOD mice with VTCN1-Ig protein significantly attenuated T1D (16). Ex vivo VTCN1 overexpression in mouse islets shielded them from T-cell cytotoxicity in transplantation experiments (17). In vivo β-cell–specific VTCN1 overexpression protected against diabetes induced by both $CD4^+$ and $CD8^+$ islet-specific clonal T cells (14,18).

All recent studies addressing the effects of VTCN1-mediated negative costimulation on the development of diabetogenic autoimmunity, however, relied on experimental models and used artificial interference and/or enhancement of VTCN1 signaling. The state of endogenous VTCN1 in T1D-susceptible animals and, most importantly, human patients, therefore, remained overlooked. Here we show that T1D pathogenesis incorporates a previously unidentified endogenous functional defect of VTCN1-mediated inhibitory costimulation, which augments the activation of diabetogenic T cells. We also demonstrate that a proteolytic cleavage by the metalloproteinase nardilysin (NRD1) is involved in VTCN1 inactivation during T1D development. Finally, we identify NRD1 as a presumptive novel therapeutic target and point out soluble VTCN1 (sVTCN1) as a potential biomarker of human T1D diagnosis.

RESEARCH DESIGN AND METHODS

Mice

Female NOD/ShiLtJ (NOD), NOD.CB17-*Prkdc*^{scid}/J (NOD-*scid*), B6.NOD-(D17Mit21-D17Mit10)/LtJ ($B6^{g7}$), and DBA/2J (DBA) mice were from The Jackson Laboratory. B6.G9C8 mice, transgenic for T-cell receptor (TCR) derived from $InsB^{15–23}$-specific $CD8^+$ T-cell clone G9C8, and *H-2K*^{d} MHC allele (19) were provided by Dr. A. Chervonsky (University of Chicago, Chicago, IL).

Human Samples

Sera from T1D cohorts, collected under institutional review board guidelines with informed consent, were from the University of Florida. Blood samples for peripheral blood mononuclear cell (PBMC) isolation were obtained according to Sanford Research institutional review board guidelines. Sera from type 2 diabetes (T2D) patients and control subjects were from BioChemed Services.

Antibodies

All antibodies and dilutions used are listed in Supplementary Table 1.

Immune Cells Isolation and Activation

Thioglycollate-elicited peritoneal macrophages were prepared as described previously (20). Bone marrow–derived macrophages (BMDMs) were generated by culturing bone marrow cells in L929-conditioned medium (21). Dendritic cells (DCs) were isolated using CD11c MicroBeads (Miltenyi Biotec). To obtain human PBMC-derived macrophages (PBMC-MΦs), leukocytes isolated from blood by Ficoll-Paque Premium (GE Healthcare) density centrifugation were adhesion enhanced and cultured for 10 days with 50 ng/mL macrophage colony-stimulating factor.

T cells were purified from NOD or B6.G9C8 spleens using Pan T Cell Isolation Kit II (Miltenyi Biotec) and labeled with carboxyfluorescein diacetate succinimidyl ester (CFSE) (22). G9C8 T cells were cocultured for 5 days with macrophages pulsed with $InsB^{15–23}$ peptide (10 μg/mL). Interleukin (IL)-2 (5 units/mL) was added on day 3. NOD T cells were cultured with NIH-3T3 (3T3) cells and activated by anti-CD3/anti-CD28–coated beads. Recombinant mouse VTCN1 or IgG was added 1 h before the beads. Medium aliquots for ELISA analysis were collected 48 h after activation. T-cell proliferation was evaluated by FACS on day 5.

Immunofluorescence

Fixed in 4% PFA, macrophages were stained for VTCN1, F4/80 or CD14, and NRD1. Cells were mounted in VECTASHIELD Mounting Medium with DAPI (Vector Laboratories) and examined under a Nikon A1 microscope. Imaging conditions were constant between all samples within an experiment. Results expressed in relative fluorescence units (RFU) were calculated for ≥100 individual cells by subtracting the mean fluorescent intensity of the control antibody from the mean fluorescent intensity of the test antibody.

FACS Analysis

Single-cell suspensions were blocked with Fc receptor antibodies (eBioscience) and were stained for VTCN1 and either F4/80 or CD14. FACS was performed on the Accuri-C6 (BD Biosciences). Data were analyzed using FlowJo software (Tree Star).

Immunoblotting

Serum-free medium conditioned by macrophages (1–3 days) was concentrated in Amicon Ultra-10K concentrators (Millipore). Macrophage lysates were prepared in radioimmunoprecipitation assay buffer, as described previously (23). Samples (7 μg protein) were subjected to immunoblot analysis using a chemiluminescent detection system. The membranes were scanned on a UVP BioSpectrum 500 imaging system.

ELISA

Mouse IL-2 and interferon-γ were analyzed using ELISA Construction Kits (Antigenix America). sVTCN1 was measured

by sandwich ELISA. Briefly, Nunc-Immuno MaxiSorp 96-well plates were coated with capturing antibodies, blocked, and incubated with sera diluted 1:10. Recombinant VTCN1 (R&D Systems) was used for standard curves. Consequent incubations with detection antibodies, horseradish peroxidase–conjugated secondary antibodies, and BioFX TMB/M substrate (SurModics) followed. Reactions were stopped with 50 μL of 1 mol/L HCl and measured at 450 nm on a SpectraMax M5 microplate reader (Molecular Devices).

RNA and cDNA

Total RNA was isolated using Direct-zol RNA MiniPrep kit (Zymo Research). RNA integrity was confirmed on 2100 Bioanalyzer (Agilent Technologies). cDNA was prepared using GoScript Reverse Transcription System (Promega).

Quantitative RT-PCR

cDNAs were amplified with gene-specific primers (Supplementary Table 2) on a Stratagene MX3005P instrument using RT^2 SYBR Green ROX qPCR Mastermix (Qiagen). Assays were normalized to multiple housekeeping genes including *β-actin* and *GAPDH*. The quantitative PCR results were analyzed by the $2^{-\Delta\Delta CT}$ method (24).

Cloning and Stable Expression of VTCN1

Full-length mouse *VTCN1* was cloned into a modified pOZ retroviral vector after PCR amplification of cDNA from NOD spleen using 5′-GGATCCATGGCTTCCTTGGGGCA GAT-3′ and 5′-CTCGAGTCATCTTAGCATCAGGCAACAG GAG-3′ as forward and reverse primers. Cloned *VTCN1* corresponded to sequences with accession numbers NM_178594 and BC032925. For truncated VTCN1 (amino acids 1–256) generation, the reverse primer 5′-CTCGAGTCAAGAGTTCAGCAACTGCAGCTG-3′, with STOP-codon before Gly257, was used. *VTCN1* sequence was integrated upstream of the puromycin-*N*-acetyltransferase gene containing an internal ribosome entry site. 3T3 cells stably expressing recombinant VTCN1 proteins were established after viral transduction and puromycin selection (25).

NRD1 Knockdown

Silencer Select small interfering RNAs (siRNAs) were from Life Technologies. A total of 2×10^5 cells were transfected with 20 nmol/L Silencer Negative Control #1 siRNA or mouse NRD1 siRNA (identification no. s106505) using Lipofectamine RNAiMAX (Life Technologies). Twenty-four hours after transfection, cells were washed and incubated for an additional 24 h in serum-free medium. The conditioned medium and cell lysates were then collected and analyzed by immunoblot.

Statistics

Group statistics were computed in GraphPad Prism (GraphPad Software). Differences between two groups were analyzed by Student *t* test. One-way ANOVA with Tukey or Dunnett post hoc test was used to analyze multiple groups. Two-way ANOVA with Bonferroni post-test was calculated for multiple effects. sVTCN1 levels within human cohorts were compared by Mann-Whitney (nonparametric) unpaired *U* test. Frequencies of "sVTCN1-positive" (sVTCN1$^+$) individuals were compared with the Fisher exact test. The correlation analyses (Figs. 1*I* and 5*G*) were based on a linear regression model with *t* statistics for parameter estimate computed in SPSS for Windows version 17 (SPSS). Nominal logistic regression analyses and standard least-squares linear models were computed using JMP software version 8 (SAS Institute).

RESULTS

Defective Surface Presentation and Elevated Shedding of VTCN1 in APCs From NOD Mice and T1D Patients

To examine the state of endogenous VTCN1 in T1D, we compared VTCN1 immunostaining of peritoneal macrophages from prediabetic and diabetic NOD mice to that of the following diabetes-resistant strains: DBA and B6^{g7}. Surface-localized VTCN1 was significantly decreased in prediabetic NOD macrophages and was nearly undetectable after the development of diabetes (Fig. 1*A*). FACS analysis of peritoneal F4/80$^+$ cells confirmed the reduction of membrane VTCN1 in diabetes-prone animals (Fig. 1*B*). A similar decline (NOD vs. B6^{g7}) was observed in BMDMs and APCs (DCs and macrophages) from pancreatic lymph nodes (Fig. 1*C* and *D* and Supplementary Fig. 1), pointing toward a generalized defect of surface VTCN1 presentation in diabetes-susceptible mice.

Gene expression analysis, however, showed a marked increase of *VTCN1* mRNA in NOD compared with B6^{g7} macrophages (Fig. 1*E*). Dissecting the discrepancy between elevated mRNA and low surface-associated VTCN1 protein levels, we found an extensive release of sVTCN1 fragment from NOD, but not DBA or B6^{g7}, macrophages (Fig. 1*F*). ELISA analysis also showed increased sVTCN1 levels in NOD compared with B6^{g7} blood sera (Fig. 1*G*), confirming that shed VTCN1 is readily detectable in vivo.

Extending our murine observations, we analyzed a small cohort of T1D patients, their first-degree relatives, and healthy age-matched control subjects for whom both sera and PBMCs were available. Obtained PBMCs were differentiated into PBMC-MΦs and used for FACS and immunofluorescence analyses (Fig. 1*H*). Measured sVTCN1 levels in sera were then correlated to the respective surface VTCN1 intensity on PBMC-MΦs (Fig. 1*I*). Similar to murine data, membrane-associated VTCN1 levels in PBMC-MΦs were significantly lower in T1D patients compared with healthy control subjects (Fig. 1*J*). Moreover, all subjects displayed a significant inverse correlation (R^2 = 0.62, P = 0.0001) between VTCN1 levels in PBMC-MΦs and sVTCN1 levels in sera, with T1D patients largely showing decreased surface and elevated sVTCN1 levels, while healthy control subjects displaying an opposite trend (Fig. 1*I*). Hence, VTCN1 shedding is driving its defective presentation in APCs from diabetes-susceptible mice and T1D patients.

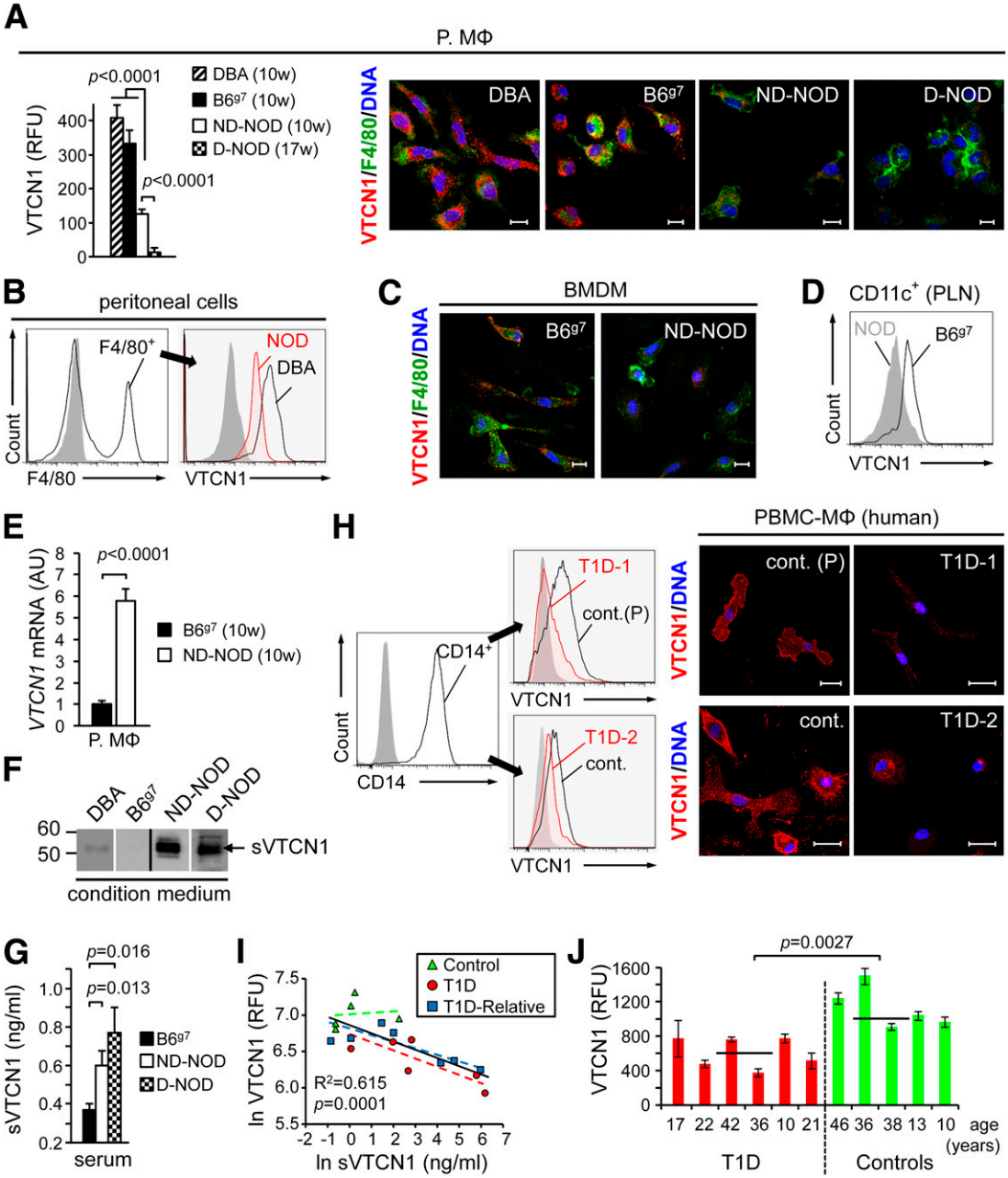

Figure 1—Surface VTCN1 presentation is altered in APCs from NOD mice and T1D patients. *A*: Quantitative analysis (*left*) and representative images (*right*) of peritoneal macrophages (P.MΦ) stained for VTCN1 (red) and F4/80 (green). Data are reported as the mean RFU ± SEM (n = 3–5 mice/group). Scale bars, 10 μm. D, diabetic; ND, nondiabetic. *B*: FACS of F4/80$^+$ peritoneal cells from mice. Gray, isotype control. *C*: Representative images of BMDMs stained as in *A*. *D*: FACS of CD11c$^+$ DCs from pancreatic lymph nodes (PLN). *E*: Quantitative RT-PCR of *VTCN1* mRNA in B6^{g7} and ND-NOD P.MΦ. Data are reported as mean arbitrary units (AU) ± SEM (n = 3 mice/group). *F*: VTCN1 immunoblot of medium conditioned by P.MΦ. Black line separates noncontiguous lanes from the same gel. *G*: ELISA of sVTCN1 in mouse sera. Data are reported as the mean ± SEM (n = 12 mice/group). *H*: FACS (*left*) and immunohistochemistry (*right*) of human CD14$^+$ PBMC-MΦs. cont.(P), nondiabetic parent of T1D-1 patient; gray, isotype control. Scale bars, 20 μm. *I*: Linear regression analysis of serum sVTCN1 and VTCN1 on PBMC-MΦs from humans. The overall correlation (solid black line) and individual correlations for each group (dashed lines of the corresponding color) are shown. *J*: Quantitative immunofluorescence analysis of VTCN1 on PBMC-MΦs from six T1D patients and five matching control subjects. Data are reported as the mean RFU ± SEM (n > 100 cells/subject). Black lines show the mean for each group. Statistics were calculated by one-way ANOVA with Tukey post hoc test (*A* and *G*) and unpaired Student t test (*E*).

Next, we investigated whether surface-associated VTCN1 deficiency can be restored by the physiological stimuli known to facilitate *VTCN1* expression (26,27). Accordingly, macrophages treated with a combination of IL-10 and transforming growth factor-β (TGF-β) increased both membrane-tethered VTCN1 and its mRNA levels (Fig. 2*A* and *B*). However, cytokine treatment had no effect on VTCN1 shedding in NOD macrophages and

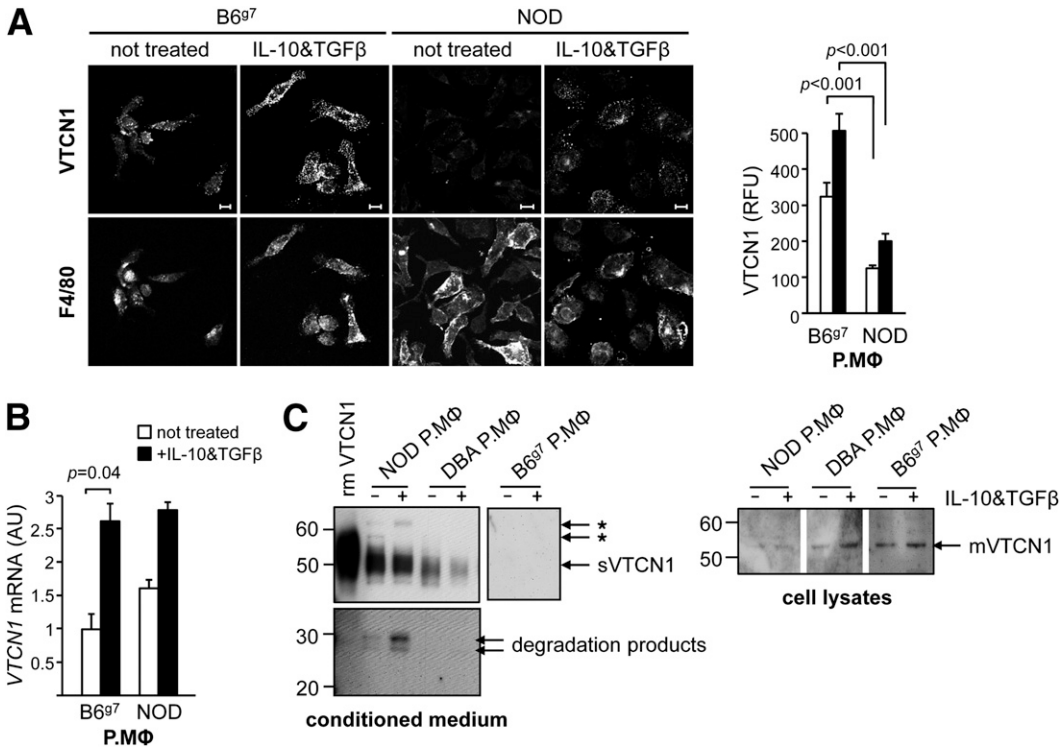

Figure 2—IL-10 and TGF-β increase VTCN1 expression and its surface presentation in peritoneal macrophages (P.MΦ). *A*: VTCN1 immunostaining of (*left*) and quantitative analysis of (*right*) the fluorescent signal F4/80$^+$ P.MΦ from B6^{g7} and prediabetic NOD mice after incubation for 72 h in the presence or absence of 10 ng/mL IL-10 and 10 ng/mL TGF-β. Scale bars, 10 μm. *B*: Quantitative RT-PCR analysis of *VTCN1* mRNA in P.MΦ treated as in *A*. Data are reported as the mean ± SEM from two experiments (n = 3 mice/group). The effect of cytokine treatment in B6^{g7} and NOD mice was evaluated by two-way ANOVA followed by Bonferroni post hoc test. *C*: Immunoblot (7 μg/lane) of conditioned medium (*left*) and cell lysates (*right*) of P.MΦ. mVTCN1, membrane-tethered VTCN1. Asterisks indicate nonspecific bands. The blot was split between 50 and 30 kD to use a darker exposure for the degraded products with lower molecular weights. AU, arbitrary units.

was insufficient in restoring their surface VTCN1 levels (Fig. 2*A* and *C*). Interestingly, cytokine treatment produced a sVTCN1 degradation product (Fig. 2*C*), suggesting that shedding compromises sVTCN1 integrity.

Loss of Surface-Associated VTCN1 Promotes Hyperproliferation of Diabetogenic T Cells

To assess VTCN1 loss during T1D development, macrophages were isolated from 5-, 10-, and 15-week-old female mice of NOD, NOD-*scid*, and B6^{g7} strains. Immunostaining revealed an age-dependent reduction of cell-associated VTCN1 in macrophages from all strains, seen most prominently in NOD and NOD-*scid* animals (Fig. 3*A*). A moderate reduction of surface VTCN1 levels in B6^{g7} macrophages was not dependent on sVTCN1 release (Fig. 3*A* and *B*) and likely relied on downregulation of mRNA expression, which declined at a similar rate (Fig. 3*C*). Conversely, a massive sVTCN1 release, accompanied by near-complete diminishment of surface-associated VTCN1, despite significant *VTCN1* mRNA upregulation, was associated with aging in NOD macrophages. Interestingly, NOD and NOD-*scid* macrophages showed similar patterns of VTCN1 loss, indicating that sVTCN1 release arises independently from lymphocyte-mediated responses.

Next, we compared the ability of B6^{g7} and NOD macrophages, loaded with exogenous insulin-derived InsB$^{15–23}$ peptide, to induce the proliferation of diabetogenic G9C8 CD8$^+$ T cells, bearing clonal InsB$^{15–23}$-recognizing TCR (19). NOD macrophages stimulated the proliferation of G9C8 cells significantly better than B6^{g7} macrophages (Fig. 3*D*). The addition of VTCN1-neutralizing antibody (28) to the B6^{g7} macrophages improved the propagation of cocultured G9C8 cells to levels achieved by NOD macrophages, confirming that VTCN1 membrane presentation is crucial for its function.

NRD1 Mediates sVTCN1 Shedding

To examine the mechanism of sVTCN1 release, we generated 3T3 cells stably expressing full-length VTCN1 (flVTCN1) or truncated, soluble VTCN1 (trVTCN1; amino acids 1–256) (Fig. 4*A*). In silico analysis using the Eukaryotic Linear Motif database (http://elm.eu.org/) revealed a potential cleavage site (K^{246}RRS^{249}), located before the transmembrane domain and predicted to be targeted by the metalloproteinase NRD1, and two subtilisin-like proprotein convertases: PCSK1 and PCSK2.

The expression of these proteinases in 3T3-based cell lines and macrophages from mice of different ages was

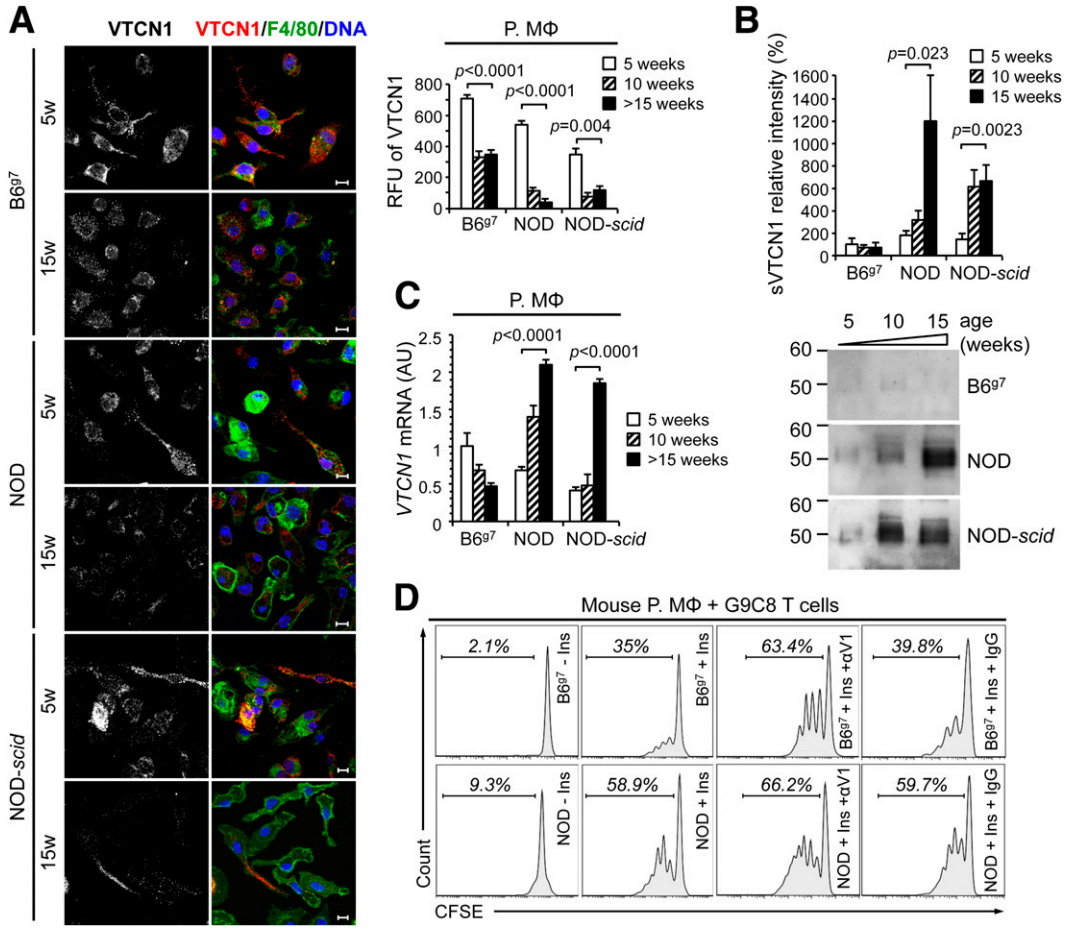

Figure 3—Shedding-dependent loss of surface VTCN1 impairs its functionality. *A*: VTCN1 immunostaining of F4/80$^+$ peritoneal macrophages (P.MΦ) isolated from B6^{g7}, NOD, and NOD-*scid* mice of indicated ages. Representative images (*left*) and quantification (*right*). Data are reported as the mean RFU ± SEM (n = 3–5 mice/group). Scale bars, 10 μm. *B*: Detection and quantification of sVTCN1 in medium conditioned by P.MΦ from B6^{g7}, NOD, and NOD-*scid* mice of different ages. Relative intensities of shed VTCN1 bands were expressed as percentages of sVTCN1 detected in media from 5-week-old B6^{g7} P.MΦ. Data are reported as the mean ± SEM (n = 4–6 group/mice). *Bottom*: Representative immunoblots. *C*: Quantitative RT-PCR analysis of *VTCN1* mRNA levels in P.MΦ from B6^{g7}, NOD, or NOD-*scid* mice at 5 and 15 weeks of age. Data are reported as the mean ± SEM (n = 3–5). *D*: FACS analysis of proliferating CFSE-labeled insulin-reactive G9C8 TCR-transgenic CD3$^+$ cells cocultured with NOD or B6^{g7} macrophages in the presence of InsB$^{15–23}$ peptide (Ins), inhibitory anti-VTCN1 antibody (αV1), or an isotype control (IgG). The percentages of proliferating cells within the gated region are shown. Statistics were calculated by one-way ANOVA with Dunnett post hoc test for each mouse strain vs. the 5-week-old group (*A* and *B*) or by two-way ANOVA (*C*).

evaluated. Substantial levels of *NRD1* and *PCSK2* mRNAs were measured in the macrophages, while only *NRD1* was expressed in 3T3 cells (Fig. 4*B* and *C*). Interestingly, both *NRD1* and *PCSK2* mRNAs gradually increased with aging in NOD and NOD-*scid* macrophages, although *PCSK2* mRNA levels decreased with age in B6^{g7} macrophages. *PCSK1* mRNA was barely detected in macrophages of all strains at any age. Because 3T3-flVTCN1 cells shed sVTCN1 (Fig. 4*D*), but lack *PCSK1* and *PCSK2* expression, these endopeptidases are likely dispensable for VTCN1 processing. Overall, these results, together with the partial colocalization of VTCN1 with NRD1 detected in permeabilized NOD macrophages (Supplementary Fig. 2), identify NRD1 as a likely VTCN1-shedding enzyme.

This prospect was further addressed using the NRD1-specific inhibitor 1,10-phenanthroline (phenanthroline) (29). Phenanthroline treatment suppressed sVTCN1 release by macrophages and 3T3-flVTCN1 cells (Fig. 4*D*). To exclude the involvement of PSCK1, PCSK2, as well as other metalloproteinases, we used a panel of inhibitors, which included the following: cathepsin/subtilisin inhibitor, known to inhibit cysteine and serine proteases; furin inhibitor II, which, alongside furin inhibition, increases PCSK2 activity; and the aminopeptidase inhibitors amastatin and bestatin, which were shown to inhibit NRD1, but not other metalloproteases (30). All three NRD1-specific inhibitors (phenanthroline, amastatin, and bestatin) constrained sVTCN1 secretion, while simultaneously stabilizing membrane VTCN1 (Fig. 4*E* and *F*). Conversely, NRD1-irrelevant cathepsin/subtilisin inhibitor and furin inhibitor II had no effect on either of these phenotypes.

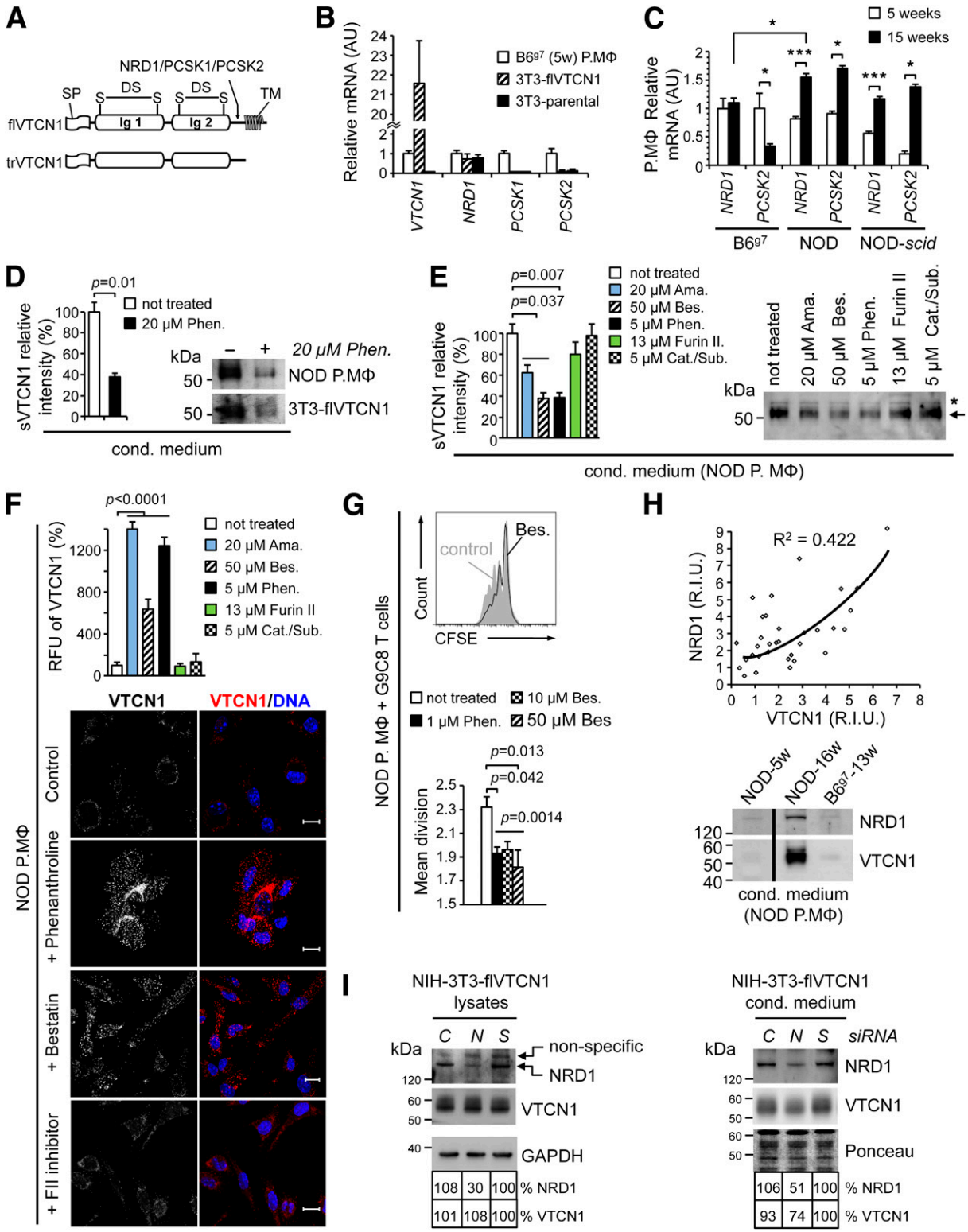

Figure 4—NRD1 cleaves cell surface VTCN1. *A*: Schematics of VTCN1. SP, signal peptide; DS, disulfide bond; TM, transmembrane domain; Ig1/2, Ig-like domains; arrow, predicted cleavage site ($K^{246}R\downarrow RS^{249}$). *B*: Quantitative RT-PCR analysis of peritoneal macrophages (P.MΦ) and 3T3 cells. Data are reported as the mean arbitrary units (AU) ± SEM (n = 3). *C*: Age-related changes in *NRD1* and *PCSK2* expression. Data are reported as the mean AU ± SEM (n = 3–5 mice/group); $^*P < 0.05$; $^{***}P < 0.001$. *D*: Detection and quantification of sVTCN1 in conditioned (cond.) medium after phenanthroline (Phen.) treatment. Data are reported as the mean ± SEM (n = 2). Representative immunoblots (*right*). *E*: Detection and quantification of sVTCN1 in conditioned medium after treatment with indicated inhibitor. Ama., amastatin; Bes., bestatin; Furin II, furin inhibitor II; Cat./Sub., cathepsin/subtilisin inhibitor. Representative immunoblot (*right*). The arrow indicates sVTCN1. The asterisk indicates a nonspecific band. Data are reported as the mean ± SEM (n = 2). *F*: Quantification (*top*) and representative images (*bottom*) of VTCN1 on P.MΦ treated with indicated inhibitor. Data are reported as the mean ± SEM (n > 100

In functional assays, treatment with NRD1 inhibitors reduced the ability of macrophages to induce $InsB^{15–23}$ peptide–dependent proliferation of G9C8 cells (Fig. 4*G*). Additionally, immunoblot analysis of media conditioned by macrophages, collected from NOD mice at different ages, showed a strong correlation between released sVTCN1 and NRD1 levels (Fig. 4*H*). Finally, *NRD1* siRNA knockdown in 3T3-flVTCN1 cells provided a considerable inhibitory effect on VTCN1 shedding (Fig. 4*I*).

Elevated Serum sVTCN1 Marks Disease in T1D Patients

To assess sVTCN1 as a potential T1D biomarker, we analyzed sera from 223 individuals: healthy control subjects (n = 74), T1D patients (n = 67), and nondiabetic first-degree relatives of T1D patients (n = 82) (Table 1). A significant 6.5-fold increase in mean sVTCN1 levels was observed in the T1D group compared with the control group (57.7 ± 14.2 and 8.9 ± 2.8 ng/mL, respectively; $P < 0.0001$; Fig. 5*A*). The mean blood sVTCN1 concentration in relatives of T1D patients (17.53 ± 5.7 ng/mL) was not significantly different from that of the control group (P = 0.5). Since T1D is largely a childhood-onset disease, the subcohort of pediatric subjects from each group was analyzed separately. Similar to the all-ages cohort, a significant 6.9-fold increase in mean sVTCN1 levels was evident in pediatric T1D patients versus control subjects (45.3 ± 13.7 and 6.6 ± 2.1 ng/mL, respectively; P = 0.001; Fig. 5*B*), while no statistical significance (P = 0.33) was observed between pediatric relatives and respective control subjects (Fig. 5*B* and Table 1). Thus, an elevated blood sVTCN1 concentration is characteristic for T1D patients of any age.

To exclude the possibility that sVTCN1 increase arises from diabetes-associated metabolic alterations unrelated to autoimmunity, we evaluated a separate cohort of T2D patients (n = 29) and respective age-, sex-, race-, and BMI-matched control subjects (n = 17) (Table 1). No significant differences in mean sVTCN1 concentrations were observed between T2D and control groups (7.8 ± 2.5 and 13.6 ± 7.8 ng/mL, respectively; P = 0.82; Fig. 5*C*), indicating that sVTCN1 marks specifically autoimmune processes.

The sVTCN1/T1D association was strengthened by nominal logistic regression analysis, which determined that log-transformed, sex- and age-adjusted sVTCN1 levels can stratify subjects from both the all-ages and pediatric cohorts for T1D diagnosis (all-ages cohort: adjusted odds ratio [OR] 1.32, $P < 0.0001$; pediatric subcohort: OR 1.31, P = 0.0002), and therefore can serve as a marker of clinically active T1D. Analysis of patients from the T2D cohort found no association of sVTCN1 levels with T2D diagnosis (OR 0.99, P = 0.59).

Next, we performed a secondary analysis, evaluating sVTCN1 levels during disease progression. Accordingly, T1D patients from the all-ages cohort were classified, based on the length of clinical disease, into either a new-onset (NO) group (<6 months from diagnosis), a 1–5 years from diagnosis group (established disease [Est]1 group), or a >5 years from diagnosis group (Est5 group) (Table 1). Control subjects were used as a reference. Strikingly, mean sVTCN1 levels did not decline alongside disease progression and remained steadily elevated in all T1D groups (NO group: 46.3 ± 23.3 ng/mL, P = 0.0001; Est1 group: 32.4 ± 16.1 ng/mL, P = 0.01; and Est5 group: 81.3 ± 26.7 ng/mL, P = 0.003; vs. control group: 8.9 ± 2.8 ng/mL; Fig. 5*D*). Multivariate regression analysis (sex and age adjusted) also did not reveal an association between log-transformed sVTCN1 concentrations and T1D duration (P = 0.4). Hence, sVTCN1 likely manifests itself rather early in the disease and persists throughout T1D.

In the context of these findings, we explored whether sVTCN1 levels rise in concert with the established autoimmune markers (anti-islet autoantibodies) or follow a separate pattern. Consequently, autoantibodies to GAD65, IA2, and zinc transporter 8 were measured (31), and pediatric T1D patients and relatives were assigned into one of the following two subgroups: autoantibody-negative (AAB^-) subjects; or subjects with an elevated titer of two or more islet-specific autoantibodies (autoantibody positive [AAB^+]). Subjects positive for one autoantibody were excluded from this secondary analysis of means. Pediatric control subjects were used as a reference. Both AAB^+ and AAB^- pediatric T1D patients exhibited prominently elevated sVTCN1 levels (AAB^+: 54.9 ± 24.2 ng/mL, P = 0.002; AAB^-: 64.5 ± 32.9 ng/mL, P = 0.066) versus the control group (6.6 ± 2.1 ng/mL; Fig. 5*E*). These levels were not significantly different from each other (P = 0.87). Similarly, the mean sVTCN1 levels in AAB^+ and AAB^- subgroups of pediatric relatives were slightly up versus control and were not significantly different from each other (Fig. 5*E* and Table 1). Nominal logistic regression analysis revealed that log-transformed, age- and sex-adjusted sVTCN1 levels were able to successfully stratify pediatric T1D patients and relatives for T1D diagnosis (OR 1.53, $P < 0.0003$), outperforming both GAD65 and IA2 autoantibodies (log transformed) as single continuous

cells/treatment). Scale bars, 10 μm. *G*: Proliferation of CFSE-labeled G9C8 cells cocultured with P.MΦ and treated with indicated inhibitor. *Top*: Representative FACS. *Bottom*: Data are reported as the mean division cycle ± SEM (n = 3). *H*: Regression analysis fit of relative immunoblot intensities of NRD1 and sVTCN1 in conditioned media from P.MΦ (*top*) and representative immunoblots (*bottom*). The black line separates noncontiguous lanes from the same gel. *I*: Immunoblots of cell lysates (*left*) and conditioned media (*right*) after siRNA silencing of NRD1. C, control; N, NRD1 siRNA; S, scrambled siRNA. Statistics were calculated by two-way ANOVA (*C*), unpaired Student *t* test (*D*), and one-way ANOVA with Dunnett post hoc test (*E–G*).

Table 1—Sample size, age, and sex distribution of study subjects

	Sample size (*n*)	Age (years)	Sex, M/F (%)	BMI	C-peptide (ng/mL)	sVTCN1 (ng/mL)	*P* value vs. control	sVTCN1$^+$ (%)	*P* value vs. control
All-ages cohort*									
Control subjects	74	21.1 ± 1.3	55/45	—	—	8.9 ± 2.8	NA	14.9	NA
T1D patients†	67	17.3 ± 1.2	51/49	—	—	57.7 ± 14.2	<0.0001	55.2	<0.0001
NO T1D	22	13.3 ± 1.5	55/45	—	0.79 ± 0.11	46.3 ± 23.3	0.0001	61.9	0.0004
Est.1 T1D	15	13.1 ± 1.0	40/60	—	BD	32.4 ± 16.1	0.01	53.3	0.003
Est.5 T1D	29	23.7 ± 2.4	55/45	—	BD	81.3 ± 26.7	0.003	58.6	<0.0001
Relatives	82	28.9 ± 2.0	54/46	—	—	17.53 ± 5.7	0.5	18.3	0.67
AAB$^+$‡	24	17.4 ± 2.8	62/38	—	—	13.8 ± 8.4	0.83	20.8	0.53
AAB$^-$	39	33.21 ± 2.5	51/49	—	—	12.6 ± 5.4	0.25	12.8	1.0
Pediatric subcohort									
Control subjects	46	14.1 ± 0.5	59/41	—	1.2 ± 0.09	6.6 ± 2.1	NA	8.7	NA
T1D patients	53	13.7 ± 0.5	55/45	—	—	45.3 ± 13.7	0.001	52.8	<0.0001
AAB$^+$‡	22	12.5 ± 0.8	55/45	—	—	54.9 ± 24.2	0.002	59.1	<0.0001
AAB$^-$	15	15.0 ± 1.0	60/40	—	—	64.5 ± 32.9	0.066	53.3	0.0006
Relatives	38	11.7 ± 0.7	61/39	—	—	14.9 ± 6.4	0.33	23.7	0.073
AAB$^+$‡	19	10.9 ± 0.9	63/37	—	—	17.1 ± 10.5	0.49	26.3	0.1
AAB$^-$	12	13.0 ± 1.5	69/31	—	—	18.9 ± 11.5	0.52	25.0	0.1
T2D cohort									
Control subjects	17	61.1 ± 4.2	53/47	25.6 ± 0.8	2.5 ± 0.4	13.6 ± 7.8	NA	17.6	NA
T2D patients	29	58.0 ± 3.3	55/45	25.2 ± 0.6	2.1 ± 0.2	7.8 ± 2.5	0.82	17.2	1.0

Data are reported as the mean ± SEM, unless otherwise indicated. BD, below detection. *The all-ages cohort does not include subjects with T2D and their respective matching control subjects. †The total number of T1D patients is higher than the sum of the respective subgroups because one patient was removed due to a lack of information about the date of blood withdrawal. ‡AAB$^+$ subpopulation includes only subjects positive for two or more autoantibodies.

variables (GAD65: OR 1.00, P = 0.35; IA2: OR 1.09, P = 0.74), and even as the GAD65/IA2 interaction term (P = 0.01) in our population. Therefore, augmentation of blood sVTCN1 likely transpires autonomously from the islet-specific antibodies and can serve as an independent indicator of T1D.

Next, we examined the frequencies of high blood sVTCN1 levels in human subjects in relation to T1D diagnosis. As the median sVTCN1 concentration in the all-ages control group was 1.1 ng/mL, we defined subjects with an ~10-fold increase of sVTCN1 concentrations (≥10 ng/mL) as sVTCN1$^+$. A total of 55.2% of all-ages T1D patients and 52.8% of pediatric T1D-diagnosed subjects were sVTCN1$^+$, which was significantly higher than the 14.9% ($P < 0.0001$) and 8.7% ($P < 0.0001$) for the respective control groups (Fig. 5*F*), suggesting that VTCN1 processing is a relevant endogenous pathway influencing a large cluster of T1D patients.

Additionally, the analysis of T1D patients grouped by the length of disease (NO, Est1, or Est5), revealed that all groups displayed a significantly higher frequency of sVTCN1$^+$ subjects (61.9%, P = 0.0004; 53.3%, P = 0.003; and 58.6%, $P < 0.0001$, respectively) versus the control group (Table 1), confirming that sVTCN1 can be considered as an early-arising, long-lasting marker of clinically active T1D.

Noticeably, autoantibody status did not affect the frequencies of sVTCN1$^+$ subjects in either pediatric T1D patients or in pediatric relatives (Fig. 5*F*), supporting our suggestion that VTCN1 shedding occurs independently from anti-islet autoantibody rise, and likely marks a separate, previously uncharacterized cluster of T1D-affected individuals.

Finally, analysis of sVTCN1$^+$ pediatric T1D patients revealed that blood sVTCN1 levels displayed a statistically significant, moderate correlation with disease aggressiveness, which was defined as the patient's age at diagnosis (R^2 = 0.3, P = 0.008; Fig. 5*G*). In contrast, sVTCN1 levels did not show a similar correlation with age in the control subject and relatives groups (Supplementary Fig. 3).

Reduced Functionality of sVTCN1 Fragment

Previous in vitro studies suggested that VTCN1 exerts inhibitory activity only in a solid surface-bound state (13). Since sVTCN1-Ig was diabetes protective in NOD mice (16), we assessed sVTCN1 activity in comparison with conventionally membrane-tethered VTCN1. sVTCN1 inhibited T-cell proliferation and cytokine production only at concentrations significantly higher than those detected in the peripheral blood of NOD mice and T1D patients (Fig. 6*A* and *B*). Because VTCN1 shedding within T-cell priming sites might result in a higher local sVTCN1 concentration, we mimicked intratissue VTCN1 discharge by coculturing activated T cells with 3T3-flVTCN1 and 3T3-trVTCN1 cell lines. In conditions of massive sVTCN1 release (occurring in both cell lines; Fig. 4*D*), membrane-bound VTCN1 on 3T3-flVTCN1 cells was notably more potent in reducing the mean division cycle of T lymphocytes than sVTCN1 produced by 3T3-trVTCN1 cells (Fig. 6*C*). The addition of recombinant sVTCN1 or VTCN1-Ig in these conditions decreased T-cell proliferation only in

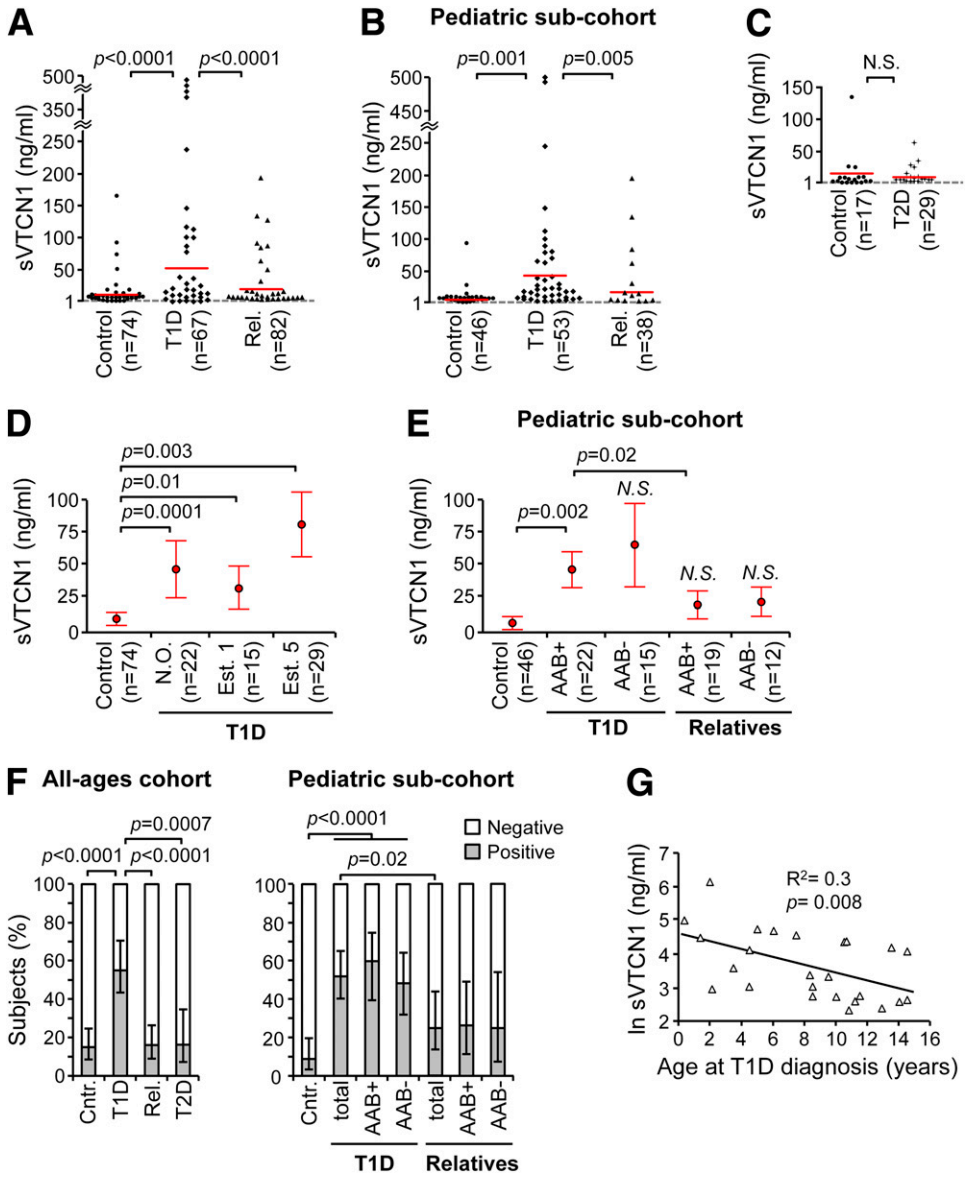

Figure 5—Elevated serum sVTCN1 levels are characteristic for T1D. *A*: Serum sVTCN1 measured by ELISA in the following three groups of patients: healthy control subjects (Control), T1D patients, and nondiabetic first-degree relatives of T1D patients (Rel.). *B*: sVTCN1 concentrations in sera from the subcohort of pediatric subjects. *C*: Serum sVTCN1 in T2D patients and their matching healthy control subjects. *A–C*: The horizontal red lines indicate the mean of the results. The *y*-axis is set up at 1 ng/mL; individual values <1 ng/mL, even though they are not shown on the graph, were included in the analysis of means. *D*: sVTCN1 levels in control subjects and T1D patients with NO of disease (<6 mo), Est1, or Est5. Data are reported as the mean ± SEM. *E*: sVTCN1 levels in a pediatric subcohort of control subjects and T1D patients, and relatives identified as AAB^- or AAB^+ for at least two islet-specific autoantibodies. Data are reported as the mean ± SEM. *F*: Frequencies (%) of $sVTCN1^-$ (<10 ng/mL) and $sVTCN1^+$ (≥10 ng/mL) subjects within the studied groups. Data are reported as the mean ± 95% CI for $sVTCN1^+$ subjects. Statistical analysis was performed by Mann-Whitney *U* test (*A–E*) and Fisher exact test (*F*). N.S., not significant. *G*: Linear regression analysis of ln-transformed sVTCN1 levels and the age at diagnosis in $sVTCN1^+$ pediatric T1D patients. The *P* value was calculated by *t* statistics for parameter estimate.

high concentrations roughly corresponding to those reported to be therapeutic in vivo in NOD mice (Fig. 6*D*).

DISCUSSION

Recent studies (9,32–36) implicate the negative costimulatory molecules B7-H1, V-domain Ig suppressor of T-cell activation, and CRIg as important players in experimental models of T1D, RA, and multiple sclerosis. Negative costimulation is generally portrayed as a mechanism limiting antigen-specific activation of autoreactive T cells. These observations triggered our study addressing the role of VTCN1 in the underlying disease mechanisms of T1D. We found that surface VTCN1 levels were remarkably reduced in NOD APCs and in PBMC-MΦs from human T1D patients (Fig. 1). In mouse macrophages, VTCN1 reduction progressed alongside disease development, occurred despite

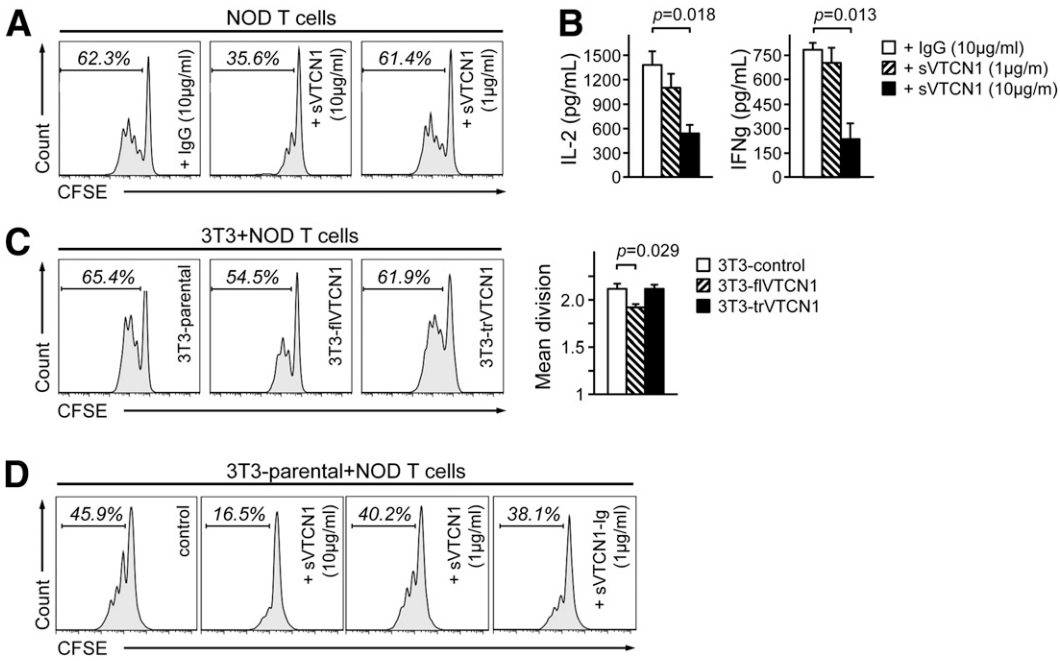

Figure 6—Functional impairment of sVTCN1 fragment. *A*: FACS analysis of proliferating CFSE-labeled NOD T cells incubated for 5 days with anti-CD3/anti-CD28–coated beads in the presence of indicated concentrations of sVTCN1 or IgG, as a nonspecific control. Percentages of proliferating T cells within the marked region are indicated. *B*: ELISA of IL-2 (*left*) and interferon-γ (*right*) secreted by activated NOD T cells 48 h after activation, as in *A*. Data are reported as the mean ± SEM ($n = 3$). *C*: FACS analysis of proliferating CFSE-labeled NOD T cells cocultured with 3T3-flVTCN1 cells or 3T3-trVTCN1 cells and activated by anti-CD3/anti-CD28–coated beads for 5 days. The 3T3 parental cell line was used as a control. Percentages of proliferating T cells within the marked region are indicated. The mean division cycle of the activated T cells is shown on the right histogram. Data are reported as the mean ± SEM ($n = 3$). *D*: FACS analysis of proliferating NOD T cells after activation with anti-CD3/anti-CD28–coated beads performed in coculture with 3T3 parental cells with or without the addition of indicated concentrations of sVTCN-Ig or sVTCN1. Percentages of proliferating T cells within the marked region are indicated. One-way ANOVA with Tukey post hoc test (*B* and *C*).

a likely compensatory increase in *VTCN1* mRNA, strongly depended on the shedding of an extracellular sVTCN1 fragment, and developed in mice with a diabetes-susceptible NOD genetic background independently of T-cell and B-cell signaling (Figs. 1 and 2). In humans, defective surface VTCN1 presentation on PBMC-MΦs was evident in T1D patients (Fig. 1*H* and *J*) and correlated with the elevated blood sVTCN1 levels (Fig. 1*I*), which were significantly higher in T1D patients compared with control subjects (Fig. 5*A* and *B*).

In a functional aspect, defective VTCN1 presentation on NOD-originated macrophages conferred hyperproliferation of diabetogenic G9C8 cells ex vivo (Fig. 3*D*). Since monocyte/macrophage recruitment initiates the formation of and drives the progression of islet infiltrates (37), VTCN1 reduction on islet-resident macrophages is likely to translate into overly aggressive insulitis and accelerated diabetes. A recent report (32) linking diabetes protection in NOD mice to the enrichment of islet infiltrates with macrophages highly expressing another coinhibitory molecule, CRIg, supports this suggestion.

Combining proteinase inhibition and gene-silencing approaches, we identified a novel pathway of VTCN1 metabolism, namely, proteolytic cleavage by NRD1 (Fig. 4), a metalloproteinase recently implicated in governing immune response via processing antigenic self-peptides (38). Reports showing elevated serum sVTCN1 levels (13) and increased *NRD1* expression in PBMCs from RA patients (39), coupled with our observations of augmented sVTCN1 in NOD mice and T1D patients (Figs. 1 and 5) and with the correlation between released sVTCN1 and NRD1 (Fig. 4*H*), suggest a fundamental proteolysis-driven impairment of VTCN1-mediated negative costimulation being associated with autoimmunity.

Concentrations of sVTCN1 detected in peripheral blood of human subjects (Fig. 5*A*–*C*) were similar to those reported in the study by Azuma et al. (13); therefore, they can be considered physiological. However, in coculture experiments sVTCN1 at such physiological levels was functionally inactive (Fig. 6*A* and *B*). Moreover, sVTCN1 was significantly less potent than membrane-tethered VTCN1 in the attenuation of T-cell proliferation (Figs. 3*D* and 6*C*). While treatment with sVTCN1-Ig protein mildly attenuated diabetes in NOD mice with a reduction from ~80% diabetes in control animals to 38% diabetes in treated mice (16), concentrations of naturally shed sVTCN1 that we detected in NOD blood were at least 150 times lower than ones used in the study by Wang et al. (16). Thus, sVTCN1 levels generated during T1D development are likely below the functional sVTCN1

threshold. Moreover, sVTCN1 appeared to be targeted for rapid degradation (Fig. 2*C*). Additionally, a recent report (13) suggested that sVTCN1 acts as a decoy for the putative VTCN1 receptor, blocking the regulatory function of membrane VTCN1. Linking sVTCN1 to the Fc portion of IgG, though, significantly improved its inhibitory activity, most probably fixing the molecule to the Fc receptors widely expressed on surface macrophages and other APCs.

The significant increase in mean blood sVTCN1 levels in T1D patients (Fig. 5*A* and *B*), coupled with the lack of significant differences in low sVTCN1 levels between T2D patients and matched control subjects (Fig. 5*C*), indicates that sVTCN1 may serve as a biomarker for autoimmune diabetes. The observed significant proportion of diabetic patients (~50%) displaying sVTCN1 positivity (Fig. 5*F*) corroborates this suggestion, and advocates that sVTCN1 can and should be further evaluated and validated as a marker of human T1D. We should not, though, exclude the possibility that the elevated sVTCN1 levels could be a general phenomenon relevant to multiple autoimmune conditions, as sVTCN1 was also reported to be elevated in RA patients (13). Further studies analyzing sVTCN1 in other autoimmune disorders should be conducted to address the question of whether changes in sVTCN1 levels are characteristic only for T1D or for autoimmunity in general.

An almost identical prominent increase in mean blood sVTCN1 levels in AAB^+ and AAB^- pediatric T1D patients, combined with the similarly identical modest elevation in sVTCN1 levels in AAB^+ and AAB^- pediatric relatives (Fig. 5*E*), together with observations of roughly equal frequencies of $sVTCN1^+$ subjects in AAB^+ and AAB^- subgroups of pediatric T1D patients, and, similarly, their first-degree relatives (Fig. 5*F*), indicated that augmentation of blood sVTCN1 is uncoupled from islet-specific antibody re sponses. Moreover, sVTCN1 clearly stratifies the pediatric population for T1D diagnosis independently of autoantibodies, therefore confirming that sVTCN1 level can serve as an autonomous and powerful marker of T1D. Human VTCN1 processing, consequently, appears to be neither associated with nor dependent on the development of anti-islet B-cell responses and, in certain similarity to NOD-*scid* mice, who lack B cells but shed VTCN1 extensively (Fig. 3*A* and *B*), is expected to mark patients who likely are harboring a predisposition for diabetogenic autoimmunity. The positioning of the *VTCN1* gene within the genomic regions associated with T1D susceptibility (*Idd10* in mouse and *Iddm26* in rat) and in immediate proximity to the human *1p13.2* T1D-susceptibility locus (www.t1Dbase.org) corroborates this hypothesis.

Our observation that sVTCN1 levels were elevated in the new-onset T1D patients (Fig. 5*D*) suggests that sVTCN1 shedding is likely initiated at the earliest disease stages and, therefore, might contribute to the conditions favoring the progression of aggressive diabetogenic autoimmunity. The direct correlation between high sVTCN1 concentrations and disease aggressiveness (Fig. 5*G*) further upholds this suggestion and indicates that sVTCN1 may be developed as a parameter for clinical T1D monitoring and for evaluation of the effectiveness of future T1D treatments.

Acknowledgments. The authors thank Drs. A. Chervonsky and V. Varnasi (University of Chicago) for transgenic B6.G9C8 mice. The authors also thank Dr. Alex Strongin (Sanford-Burnham Institute), and Drs. Satoshi Nagata and Olga Savinova (Sanford Research) for their valuable comments and thoughts; Dr. Susan Puumala (Sanford Research) for her advice on the statistical analyses; and Jens Saakvitne, Ryan Dott, Cody Belitz, and the staff of South Dakota Lions Eye and Tissue Bank for help in obtaining human tissues. The authors thank the Sanford Research Imaging and Flow Cytometry Core facilities for their service.

Funding. This work was supported by the Sanford Research start-up funds and JDRF research grants 26-2008-876 and 47-2013-522 to A.Y.S. The Sanford Research Imaging and Flow Cytometry Core facilities were partially supported by National Institutes of Health COBRE grant 1P20RR024219.

Duality of Interest. No potential conflicts of interest relevant to this article were reported.

Author Contributions. I.A.R. contributed to the design of the experiments; performed the inhibitors studies, in vitro T-cell activation, immunofluorescence, and ELISA; executed the RNA analysis; helped to analyze the data; and wrote the manuscript. L.V.M.-R. performed the inhibitor studies, in vitro T-cell activation, immunofluorescence, and ELISA. C.A. executed the RNA analysis. C.P. completed the FACS analysis, helped to analyze the data, and contributed to the writing of the manuscript. J.E. and M.A. contributed to the writing of the manuscript. C.W. contributed to human serum studies. P.B. contributed to the design of the experiments. A.Y.S. contributed to the design of the experiments, helped to analyze the data, and contributed to the writing of the manuscript. A.Y.S. is the guarantor of this work and, as such, had full access to all the data in the study and takes responsibility for the integrity of the data and the accuracy of the data analysis.

References

1. La Torre D, Lernmark A. Immunology of beta-cell destruction. Adv Exp Med Biol 2010;654:537–583

2. Haskins K, Cooke A. CD4 T cells and their antigens in the pathogenesis of autoimmune diabetes. Curr Opin Immunol 2011;23:739–745

3. Danke NA, Koelle DM, Yee C, Beheray S, Kwok WW. Autoreactive T cells in healthy individuals. J Immunol 2004;172:5967–5972

4. Fink PJ, Hendricks DW. Post-thymic maturation: young T cells assert their individuality. Nat Rev Immunol 2011;11:544–549

5. Bach JF, Chatenoud L. Tolerance to islet autoantigens in type 1 diabetes. Annu Rev Immunol 2001;19:131–161

6. Fife BT, Bluestone JA. Control of peripheral T-cell tolerance and autoimmunity via the CTLA-4 and PD-1 pathways. Immunol Rev 2008;224:166–182

7. Dong H, Zhu G, Tamada K, Chen L. B7-H1, a third member of the B7 family, co-stimulates T-cell proliferation and interleukin-10 secretion. Nat Med 1999;5:1365–1369

8. Sica GL, Choi IH, Zhu G, et al. B7-H4, a molecule of the B7 family, negatively regulates T cell immunity. Immunity 2003;18:849–861

9. Wang L, Rubinstein R, Lines JL, et al. VISTA, a novel mouse Ig superfamily ligand that negatively regulates T cell responses. J Exp Med 2011;208:577–592

10. Prasad DV, Richards S, Mai XM, Dong C. B7S1, a novel B7 family member that negatively regulates T cell activation. Immunity 2003;18:863–873

11. Wang X, Hao J, Metzger DL, et al. B7-H4 Treatment of T Cells Inhibits ERK, JNK, p38, and AKT Activation. PLoS One 2012;7:e28232

12. Zang X, Loke P, Kim J, Murphy K, Waitz R, Allison JP. B7x: a widely expressed B7 family member that inhibits T cell activation. Proc Natl Acad Sci U S A 2003;100:10388–10392

13. Azuma T, Zhu G, Xu H, et al. Potential role of decoy B7-H4 in the pathogenesis of rheumatoid arthritis: a mouse model informed by clinical data. PLoS Med 2009;6:e1000166
14. Wei J, Loke P, Zang X, Allison JP. Tissue-specific expression of B7x protects from CD4 T cell-mediated autoimmunity. J Exp Med 2011;208:1683–1694
15. Ou D, Wang X, Metzger DL, et al. Suppression of human T-cell responses to beta-cells by activation of B7-H4 pathway. Cell Transplant 2006;15:399–410
16. Wang X, Hao J, Metzger DL, et al. Early treatment of NOD mice with B7-H4 reduces the incidence of autoimmune diabetes. Diabetes 2011;60:3246–3255
17. Wang X, Hao J, Metzger DL, et al. Local expression of B7-H4 by recombinant adenovirus transduction in mouse islets prolongs allograft survival. Transplantation 2009;87:482–490
18. Lee JS, Scandiuzzi L, Ray A, et al. B7x in the periphery abrogates pancreas-specific damage mediated by self-reactive CD8 T cells. J Immunol 2012;189:4165–4174
19. Varanasi V, Avanesyan L, Schumann DM, Chervonsky AV. Cytotoxic mechanisms employed by mouse T cells to destroy pancreatic β-cells. Diabetes 2012;61:2862–2870
20. Zhang X, Goncalves R, Mosser DM. The isolation and characterization of murine macrophages. Curr Protoc Immunol 2008;Chapter 14:Unit 14.1
21. Walker EB, Akporiaye ET, Warner NL, Stewart CC. Characterization of subsets of bone marrow-derived macrophages by flow cytometry analysis. J Leukoc Biol 1985;37:121–136
22. Lyons AB, Parish CR. Determination of lymphocyte division by flow cytometry. J Immunol Methods 1994;171:131–137
23. Radichev IA, Remacle AG, Shiryaev SA, et al. Biochemical characterization of the cellular glycosylphosphatidylinositol-linked membrane type-6 matrix metalloproteinase. J Biol Chem 2010;285:16076–16086
24. Livak KJ, Schmittgen TD. Analysis of relative gene expression data using real-time quantitative PCR and the 2(-Delta Delta C(T)) method. Methods 2001;25:402–408
25. Radichev I, Kwon SW, Zhao Y, DePamphilis ML, Vassilev A. Genetic analysis of human Orc2 reveals specific domains that are required in vivo for assembly and nuclear localization of the origin recognition complex. J Biol Chem 2006;281:23264–23273
26. Cao Q, Wang Y, Zheng D, et al. IL-10/TGF-beta-modified macrophages induce regulatory T cells and protect against adriamycin nephrosis. J Am Soc Nephrol 2010;21:933–942
27. Kryczek I, Wei S, Zou L, et al. Cutting edge: induction of B7-H4 on APCs through IL-10: novel suppressive mode for regulatory T cells. J Immunol 2006;177:40–44
28. Yamaura K, Watanabe T, Boenisch O, et al. In vivo function of immune inhibitory molecule B7-H4 in alloimmune responses. Am J Transplant 2010;10:2355–2362
29. Hospital V, Chesneau V, Balogh A, et al. N-arginine dibasic convertase (nardilysin) isoforms are soluble dibasic-specific metalloendopeptidases that localize in the cytoplasm and at the cell surface. Biochem J 2000;349:587–597
30. Chesneau V, Pierotti AR, Barré N, Créminon C, Tougard C, Cohen P. Isolation and characterization of a dibasic selective metalloendopeptidase from rat testes that cleaves at the amino terminus of arginine residues. J Biol Chem 1994;269:2056–2061
31. Cambuli VM, Incani M, Cossu E, et al. Prevalence of type 1 diabetes autoantibodies (GADA, IA2, and IAA) in overweight and obese children. Diabetes Care 2010;33:820–822
32. Fu W, Wojtkiewicz G, Weissleder R, Benoist C, Mathis D. Early window of diabetes determinism in NOD mice, dependent on the complement receptor CRIg, identified by noninvasive imaging. Nat Immunol 2012;13:361–368
33. Katschke KJ Jr, Helmy KY, Steffek M, et al. A novel inhibitor of the alternative pathway of complement reverses inflammation and bone destruction in experimental arthritis. J Exp Med 2007;204:1319–1325
34. Keir ME, Liang SC, Guleria I, et al. Tissue expression of PD-L1 mediates peripheral T cell tolerance. J Exp Med 2006;203:883–895
35. Nishimura H, Nose M, Hiai H, Minato N, Honjo T. Development of lupus-like autoimmune diseases by disruption of the PD-1 gene encoding an ITIM motif-carrying immunoreceptor. Immunity 1999;11:141–151
36. Salama AD, Chitnis T, Imitola J, et al. Critical role of the programmed death-1 (PD-1) pathway in regulation of experimental autoimmune encephalomyelitis. J Exp Med 2003;198:71–78
37. Gaglia JL, Guimaraes AR, Harisinghani M, et al. Noninvasive imaging of pancreatic islet inflammation in type 1A diabetes patients. J Clin Invest 2011;121:442–445
38. Kessler JH, Khan S, Seifert U, et al. Antigen processing by nardilysin and thimet oligopeptidase generates cytotoxic T cell epitopes. Nat Immunol 2011;12:45–53
39. Teixeira VH, Olaso R, Martin-Magniette ML, et al. Transcriptome analysis describing new immunity and defense genes in peripheral blood mononuclear cells of rheumatoid arthritis patients. PLoS One 2009;4:e6803